Mechanism of nonvolatile resistive switching in graphene oxide thin films

Fei Zhuge, Benlin Hu, Congli He, Xufeng Zhou, Zhaoping Liu, Run-Wei Li *

Key Laboratory of Magnetic Materials and Devices, Ningbo Institute of Materials Technology and Engineering, Chinese Academy of Sciences, Ningbo 315201, China

Zhejiang Province Key Laboratory of Magnetic Materials and Application Technology, Ningbo 315201, China

A R T I C L E   I N F O

A B S T R A C T

The mechanism of the resistive switching (RS) effect in graphene oxide (GO) thin films prepared by the vacuum filtration method has been investigated by macroscopic current–voltage (I–V) measurements and conducting atomic force microscopy (CAFM). Detailed I–V measurements show that in metal/GO/Pt sandwiches, the RS originates from the formation and rupture of conducting filaments. An analysis of the temperature dependence of the ON-state resistance reveals that the filaments are composed of metal atoms due to the diffusion of the top electrodes under a bias voltage. Moreover, the RS is found to occur within confined regions of the metal filaments. The RS effect is also observed in GO/Pt structures by CAFM. It is attributed to the redox reactions between GO and adsorbed water induced by external voltage biases.

1.   Introduction

Resistive random access memory (RRAM) based on the resistive switching (RS) effect induced by electrical stimulus has inspired scientific and commercial interests due to its high operation speed, high scalability, and multibit storage potential [1–3]. The reading of resistance states is nondestructive, and the memory devices can be operated without transistors in every cell [4,5], thus making a cross-bar structure feasible. A large variety of solid-state materials have been found to exhibit the RS effect, including solid electrolytes [5], complex perovskite oxides [1,6–10], binary oxides [11–18], organic materials [19], amorphous silicon [20], and amorphous carbon [21,22]. Graphene oxide (GO) with an ultrathin thickness (∼1 nm) is attractive due to its unique physical–chemical properties. GO can be readily obtained through oxidizing graphite in mixtures of strong oxidants, followed by an exfoliation process. Due to its water solubility, GO can be transferred onto any substrates uniformly using simple methods such as drop-casting, spin coating, Langmuir–Blodgett deposition and vacuum filtration. The as-deposited GO thin films can be further processed into functional devices using standard lithography processes without degrading the film properties [23,24]. Furthermore, the band structure and electronic properties of GO can be modulated by changing the quantity of chemical functionalities attached to the surface. Therefore, GO is a promising material for microelectronic devices, for example RRAM. The water solubility makes it very easy to form GO thin films and the ultrathin thickness of a GO sheet is beneficial to fabricating high density devices. Recently, we observed reliable and reproducible nonvolatile RS behaviors in GO thin films prepared by the vacuum filtration method [25]. At a later time, the similar RS phenomena were also observed in GO films prepared by spin-casting and conjugated-polymer-functionalized GO [26–29]. However, the mechanism responsible for the RS effect of GO is still not clear. In this paper, the mechanism of the RS effect in GO thin films has been investigated by macroscopic current–voltage

(*I–V*) measurements and conducting atomic force microscopy (CAFM) in detail.

2. Experimental

2.1. Preparation of GO thin films

GO thin films of about 30 nm in thickness were prepared at room temperature (RT) by the vacuum filtration method as described in Ref. [25]. First we obtained GO suspensions through the soft-chemical delamination of GOs as described in Ref. [30] (see the Supporting Information). Then 50 g of GO suspension with a concentration of 6 mg/L was filtered through a cellulose ester membrane to achieve uniform GO thin films. The film thickness could be well controlled by tuning the GO concentration or filtration volume. The as-filtered GO flakes were then transferred from the filter membrane onto commercial Pt/Ti/SiO$_2$/Si substrates.

2.2. Characterizations

Atomic force microscopy (AFM) characterization was conducted by a Veeco Dimension 3100 V scanning probe microscope at ambient conditions using a tapping or CAFM mode. In order to measure the electrical properties, metal (Cu, Ag, Au and Ti) top electrodes with a thickness of 200 nm and diameter of 100 μm were deposited at RT by electron beam evaporation with an in situ metal shadow mask. The *I–V* characteristics of metal/GO/Pt structures were measured at RT by Keithley 4200 semiconductor characterization system with voltage sweeping mode. During the measurement, a bias voltage was applied between the top (Cu, Ag, Au and Ti) and bottom (Pt) electrodes with the latter being grounded. In the local leakage current measurement by CAFM, the Pt/Ir coated conductive tip was grounded and directly touched the GO films. Schematic configurations of the metal/GO/Pt sandwiched structures and for the CAFM measurements are show in Fig. S1 in the Supporting Information. The resistances in the low resistance state (LRS or ON state) and high resistance state (HRS or OFF state) of the metal/GO/Pt structures were measured as a function of temperature by a physical property measurement system (PPMS, Quantum Design).

3. Results and discussion

3.1. RS mechanism in metal/GO/Pt sandwiches

Metal/GO/Pt sandwiched structures show the bipolar RS behaviors as described in Ref. [25] (see Fig. S2 in the Supporting Information). To understand the conduction mechanisms of metal/GO/Pt memory cells, the *I–V* curves of the Cu/GO/Pt structure are replotted in a log–log scale. Fig. 1a and b shows the logarithmic plot and linear fitting of the *I–V* curves for the positive and negative voltage sweep regions, respectively, where the SET process is the switching from HRS to LRS and the RESET process is the switching from LRS to HRS. As shown in Fig. 1, the *I–V* curves of the LRS exhibit a linearly Ohmic behavior with a slope of ~1. However, the conduction mechanisms of HRS are more complicated. Fitting results

for the HRS suggest that the charge transport behavior is in good agreement with a trap-controlled space charge limited conduction (SCLC), which mainly consists of two portions: the Ohmic region ($I \propto V$) and the Child's law region ($I \propto V^2$) [31,32]. The different conduction behaviors in the HRS and LRS suggest that the high conductivity in ON-state cell is likely to be a confined effect rather than a homogenously distributed one [18].

Actually, a Forming process, which is the first transition from fresh state to LRS, is always needed before metal/GO/Pt sandwiches show good RS characteristics. Fig. 2a shows the GO film thickness dependence of Forming voltages of Cu/GO/Pt memory cells. Obviously, the voltage required for the initial Forming process increases with GO thickness, indicating that the electric field inside the bulk GO is the controlling factor of the Forming. The resistances of HRS and LRS after the Forming process for Cu/GO/Pt memory cells are shown in Fig. 2b, as a function of the thickness of GO. No obvious variation can be observed for both HRS and LRS resistances as the GO thickness changes from 15 to 90 nm. The thickness-insensitive property of HRS and LRS resistances indicates that once the Forming process is completed, it is unlikely that the bulk region of GO contributes to the RS effectively [33]. Most likely, the RS occurs within a spatially confined region.

Fig. 3a shows the Forming voltages of metal/GO/Pt memory cells with different top electrodes. As seen from Fig. 3a, the Ag/GO/Pt structures have the lowest Forming voltages of about 0.4 V, while the Au/GO/Pt sandwiches show the highest Forming voltages of about 3 V. The Forming voltage of the metal/GO/Pt memory cell varies as follows: $V_{Ag} < V_{Ti} < V_{Cu} < V_{Au}$. Fig. 3b shows the top electrode dependence of device yields of metal/GO/Pt memory cells. More than one hundred cells were examined for each sample. As can be seen from Fig. 3b, the device yield (Y) of the metal/GO/Pt memory cell varies as follows: $Y_{Ag} > Y_{Cu} > Y_{Au} > Y_{Ti}$. The Ag/GO/Pt structure has the highest device yield of about 70%. The strong top electrode material dependence of the switching characteristics is helpful for speculating about the RS mechanism in metal/GO/Pt devices. Tokunaga et al. investigated the RS effect at the interface between metal electrodes (Pt, Au, Ag, Al, Ti, and Mg) and atomically flat cleaved (001) surfaces of La$_{1-x}$Sr$_{1+x}$MnO$_4$ ($x = 0$–1.0) single crystals [34]. Hysteretic *I–V* characteristics were observed in the junctions for Mg, Al, and Ti, which have relatively shallow work functions (Φ). In our case, Ti, Cu, and Ag have a lower Φ of 3.98, 4.35 and 4.26 eV, respectively, whereas Au has a higher one of 5.1 eV. It indicates that the occurrence of the RS in metal/GO/Pt structures is irrelevant to Φ of the top electrodes. Liao and co-workers studied the RS characteristics of metal/Pr$_{0.7}$Ca$_{0.3}$MnO$_3$/Pt devices and found that devices with top electrode made of Al, Ti, and Ta exhibit a bipolar resistive switching, but those with top electrode made of Pt, Ag, Au, and Cu do not [8]. The RS was attributed to a thin metal-oxide layer formed at the interface between the former group of top electrode and Pr$_{0.7}$Ca$_{0.3}$MnO$_3$. In our work, the top electrode material includes both reactive metals such as Ti and inert metals such as Au. Therefore, the observed RS is not due to the formation of a metal-oxide layer at the interface between the top electrode and GO. It has been reported that solid electrolyte memory devices based on silver ions
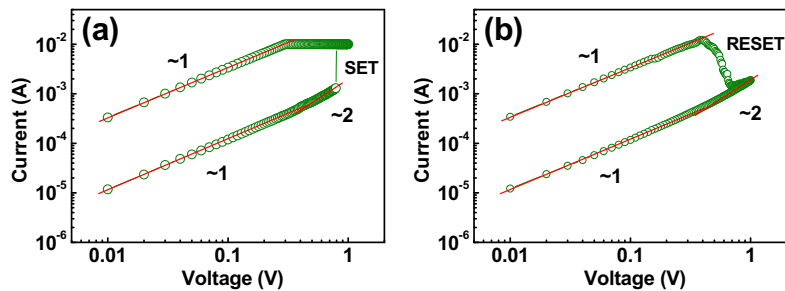
Fig. 1 – *I–V* curves of the Cu/GO/Pt memory cell plotted in log–log scale and the linear fitting results in both LRS and HRS: (a) positive voltage region and (b) negative voltage region. Also shown are the corresponding slopes for different portions.
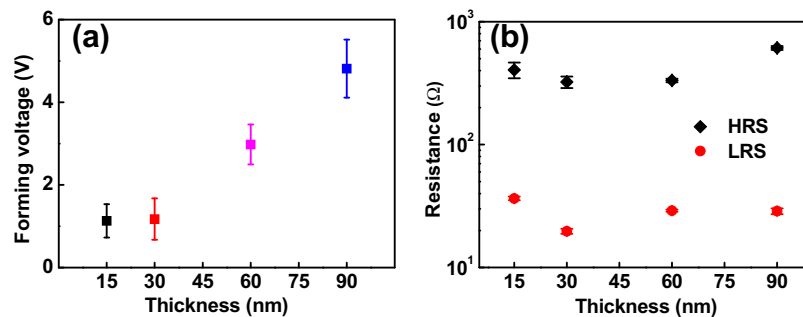
Fig. 2 – (a) GO film thickness dependence of Forming voltage of Cu/GO/Pt memory cells. (b) Resistances of HRS and LRS for Cu/GO/Pt memory cells, plotted against the thickness of GO.
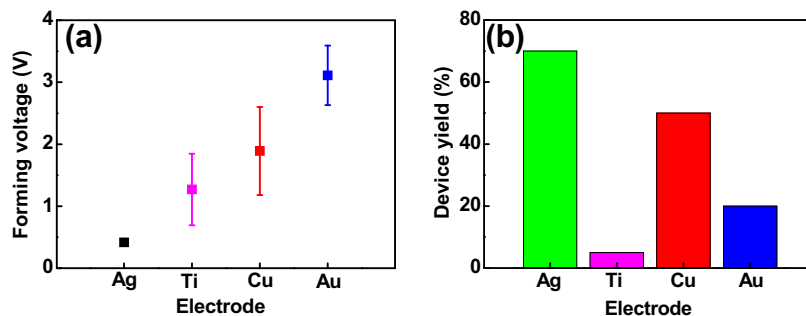
Fig. 3 – (a) Forming voltages and (b) device yields of different metal/GO/Pt sandwiches.

generally show low switching voltages [35–37]. Banno et al. further clarified that the switching voltage for turn-on in RRAM devices based on solid electrolyte such as $Cu_{2-z}S$ and Ta_2O_5 could be strongly affected by the ion flux which is proportional to the product of the diffusion coefficient and the concentration of ions [38]. Therefore, we can infer that a large ion diffusion coefficient can lead to a large ion flux and thus a low switching voltage. Govindaraj et al. have reported that Ag has a large diffusion coefficient in oxide films [39]. The Ag/ZrO₂/Au structure shows low switching voltages of <1 V without any Forming process [40]. In our case, it is likely that Ag also has a large diffusion coefficient in GO thin films, resulting in low Forming voltages for Ag/GO/Pt memory cells. The high Forming voltages for Au/GO/Pt structures are likely due to gold's chemical inertness. Compared to other top electrode metals (Ag, Ti, and Cu), gold is very difficult to be oxidized to the ions. High voltages are necessary for the activation of Au/

GO/Pt memory cells. From the analysis above, we infer that the RS effect in metal/GO/Pt memory cells is attributed to the formation/rupture of metal filaments due to the diffusion of the top electrodes under a bias voltage. Briefly, a positive voltage (>SET voltage) on the top electrodes generates a high electric field that drives metal (e.g., Ag) ions into the GO matrix and form conducting filaments inside the GO layer, and the device reaches the ON state. After the SET process, the device retains the ON state unless a sufficient voltage of opposite polarity (<RESET voltage) is applied and the electrochemical dissolution of the metal filaments RESETs the device, and the OFF state is finally reached again [20,22].

To verify the physical nature of the RS effect in metal/GO/Pt structures, resistances in the low and high resistance states of the Cu/GO/Pt device are measured as a function of temperature (*T*). Fig. 4a shows the typical metallic behavior of the resistance in the ON state. In contrast, the resistance in the
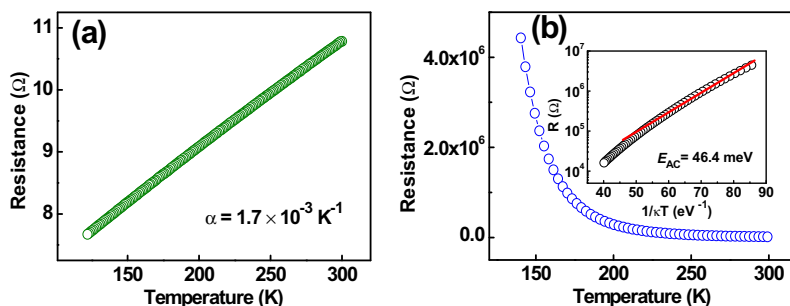
Fig. 4 – (a) Temperature dependence of the resistance in LRS of the Cu/GO/Pt device. Also shown is the temperature coefficient of resistance (α) of the conducting filaments. (b) Temperature dependence of the resistance in HRS. The inset shows the Arrhenius plot of the resistance and calculated activation energy (E_{AC}) for conduction.

OFF state shows a semiconducting behavior as displayed in Fig. 4b. The resistance (R) decreases with T, according to the Arrhenius law: $R(T) = R_A\exp(E_{AC}/\kappa T)$, where R_A is the Arrhenius preexponential factor for resistance, E_{AC} is the activation energy for conduction, and κ is the Boltzmann constant. The inset of Fig. 4b shows the Arrhenius plot of the HRS resistance, from which E_{AC} is calculated to be 46.4 meV. The metallic conducting behavior in LRS indicates the formation of conducting filaments in GO films [22]. The temperature dependence of metallic resistance can be written as $R(T) = R_0[1 = \alpha(T - T_0)]$, where R_0 is the resistance at temperature T_0, and α is the temperature coefficient of resistance. By choosing T_0 as 300 K, the temperature coefficient of resistance of the filaments is calculated to be 1.7×10^{-3} K^{-1}, which is close to the value 2.5×10^{-3} K^{-1} for high-purity copper nanowires of diameter $\geqslant 15$ nm [41], confirming that the filaments are composed of Cu in metallic states due to the diffusion of the top electrode under a bias voltage. The discrepancy of the

temperature coefficient of resistance is attributed to inevitable defects in the Cu filaments, since the presence of defects can reduce the temperature coefficient of resistance by shortening the mean free path of electrons [41]. Therefore, the origin of the RS in metal/GO/Pt memory cells is the formation/rupture of metal filaments due to the diffusion of the top electrodes under a bias voltage, as schematically illustrated in Fig. S3 in the Supporting Information. As seen from Fig. 3b, the Ti/GO/Pt structures have the lowest device yield (Y < 10%). It is likely due to the formation of a thin TiO$_x$ layer at the interface between the top electrode and GO which is detrimental to the Ti ion diffusion. Although the Forming voltage and device yield of metal/GO/Pt devices show a strong dependence on the top electrode material, the memory devices with different top electrodes show good retention and endurance properties, as described in Figs. S4 and S5 in the Supporting Information, respectively. It indicates that for metal/GO/Pt memory cells the switching behavior will be stable
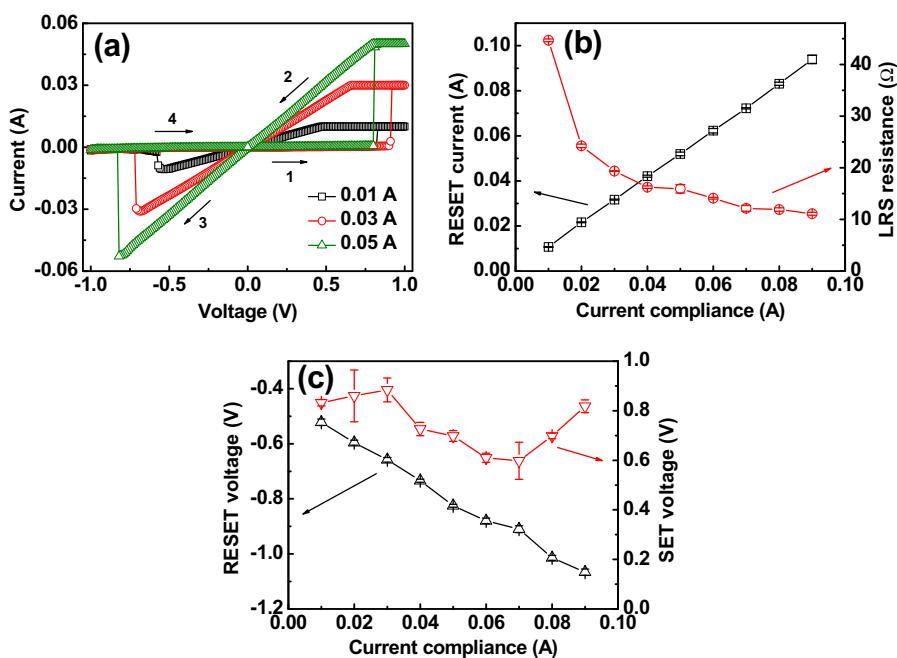
Fig. 5 – (a) Typical I–V characteristics of the Cu/GO/Pt device with different current compliance (0.01, 0.03 and 0.05 A). (b) Current compliance dependence of the RESET current and LRS resistance of the Cu/GO/Pt device. (c) Current compliance dependence of the SET and RESET voltages of the Cu/GO/Pt device.
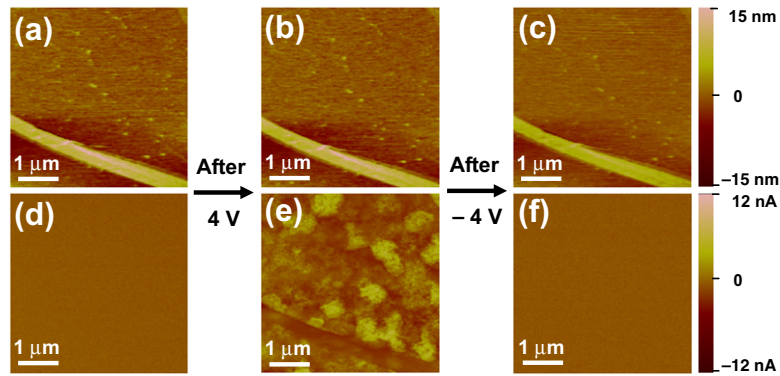
Fig. 6 – (a), (b) and (c) AFM images of virgin GO films, GO films in LRS, and GO films in HRS. The light-colored ribbons represent folded regions. (d), (e) and (f) the corresponding CAFM images under a read voltage of 1 V.

once the metal filaments completely form, regardless of the top electrode material. Note that ON/OFF ratios (R_{OFF}/R_{ON}) of Cu/GO/Pt devices shown in Figs. S4 and S5 are much higher than that in Fig. S2. Considering that the I–V measurements were performed in air and the data in Figs. S2, S4 and S5 were obtained at different times with large humidity variation, it is likely that the moisture in air affects the ON/OFF ratio of metal/GO/Pt memory cells severely.

A current compliance is usually needed during the Forming and SET processes to prevent the sample from a permanent breakdown. Current compliance is another critical parameter to determine the RS characteristics of metal/GO/Pt memory cells. Employing the filament model, it is easy to understand the current compliance dependence of the RS characteristics in metal/GO/Pt sandwiches, as shown in Fig. 5. Fig. 5a shows the typical I–V characteristics of the Cu/GO/Pt device with different current compliance (0.01, 0.03 and 0.05 A). Clearly, the RESET current (maximum current level before the RESET process) increases with current compliance. The dependence of the RESET current and LRS resistance on current compliance applied in the SET process is shown in Fig. 5b. The RESET current has an approximate linear relationship to the current compliance. The resistance in LRS decreases with increasing current compliance. Fig. 5c shows the current compliance dependence of the SET and RESET voltages. The SET voltage shows weak dependence on current compliance, whereas the RESET voltage increases with current compliance. It is considered that stronger filaments with a higher density are formed at a larger current compliance, resulting in a lower LRS resistance [42]. The RESET process is due to the rupture of the filaments due to the electrochemical dissolution. Thus, it can be imagined that a larger voltage or a larger current is necessary for the RESET process at a larger current compliance.

3.2. RS mechanism in GO/Pt structures

CAFM was used to study the RS phenomenon in GO/Pt structures. The Pt/Ir coated conducting tip was grounded and directly touched the GO films. The voltage was applied to the bottom electrode (Pt). CAFM measurements were performed in the same region of 5×5 μm^2 in size under various external voltage biases, as shown in Fig. 6. From Fig. 6d, we can see that

the virgin GO is in HRS, which is switched to LRS after applying a positive voltage of 4 V, as shown in Fig. 6e. The sample can be switched back to HRS by applying a negative voltage of 4 V, as shown in Fig. 6f. The similar RS phenomenon could also be observed in a much smaller region of 200×200 nm^2 (see Fig. S6 in the Supporting Information). As seen from Fig. 6, the LRS current should not flow through the filamentary conduction paths which are confined within nanoscale regions [18]. Zhou et al. reported that hydrogen ions play an essential role in electrochemical GO reduction [43]. Considering that the CAFM measurements were performed in air with a relative humidity level of about 60%, a several-monolayer-thick water layer readily adsorbs on hydrophilic surfaces. Therefore, when the CAFM tip is in contact with GO, a water meniscus forms around the tip and acts as a localized electrochemical environment. It is likely that when applying a positive voltage, the water layer at the tip/GO interface is oxidized, thereby generating hydrogen ions that take part in reducing the GO [44]. The reduction of GO results in the resistance switching from HRS to LRS. While applying a negative voltage, the reduced GO is oxidized again [45], switching the sample back to HRS. Therefore, the redox reactions between GO sheets near the film surface and adsorbed water induced by external voltage biases lead to the RS effect in GO/Pt structures.

4. Summary

We have investigated the resistive switching mechanism in metal/GO/Pt and GO/Pt structures by macroscopic I–V measurements and CAFM. The results demonstrate that the RS in metal/GO/Pt sandwiches is due to the formation/rupture of conducting filaments composed of metal atoms from the diffusion of the top electrodes under a bias voltage. Furthermore, the RS is found to occur within confined regions of the filaments. The origin of the RS observed in GO/Pt structures by CAFM is the redox reactions between GO and adsorbed water induced by external voltage biases.

Acknowledgments

Appendix A.   Supplementary data

Supplementary data associated with this article can be found, in the online version, at doi:10.1016/j.carbon.2011.04.071.

REFERENCES

[1] Beck A, Bednorz JG, Gerber C, Rosse CL, Widmer D. Reproducible switching effect in thin oxide films for memory applications. Appl Phys Lett 2000;77(1):139–41.

[2] Lu W, Lieber CM. Nanoelectronics from the bottom up. Nat Mater 2007;6(11):841–50.

[3] Dong Y, Yu MG, McAlpine C, Lu W, Lieber CM. Si/α-Si core/shell nanowires as nonvolatile crossbar switches. Nano Lett 2008;8(2):386–91.

[4] Lee MJ, Park Y, Suh DS, Lee EH, Seo S, Kim DC, et al. Two series oxide resistors applicable to high speed and high density nonvolatile memory. Adv Mater 2007;19(22):3919–23.

[5] Waser R, Aono M. Nanoionics-based resistive switching memories. Nat Mater 2007;6(11):833–40.

[6] Liu SQ, Wu NJ, Ignatiev A. Electric-pulse-induced reversible resistance change effect in magnetoresistive films. Appl Phys Lett 2000;76(19):2749–51.

[7] Odagawa A, Sato H, Inoue IH, Akoh H, Kawasaki M, Tokura Y. Colossal electroresistance of a $Pr_{0.7}Ca_{0.3}MnO_3$ thin film at room temperature. Phys Rev B 2004;70:224403 (22).

[8] Liao ZL, Wang ZZ, Meng Y, Liu ZY, Gao P, Gang JL, et al. Categorization of resistive switching of metal-$Pr_{0.7}Ca_{0.3}MnO_3$–metal devices. Appl Phys Lett 2009;94(25):253503.

[9] Yin KB, Li M, Liu YW, He CL, Zhuge F, Chen B, et al. Resistance switching in polycrystalline $BiFeO_3$ thin films. Appl Phy Lett 2010;97(4):042101.

[10] Li M, Zhuge F, Zhu XJ, Yin KB, Wang JZ, Liu YW, et al. Nonvolatile resistive switching in metal/La-doped $BiFeO_3$/Pt sandwiches. Nanotechnology 2010;21(42):425202.

[11] Seo S, Lee MJ, Seo DH, Jeoung EJ, Suh DS, Joung YS, et al. Reproducible resistance switching in polycrystalline NiO films. Appl Phys Lett 2004;85(23):5655–7.

[12] Son JY, Shin YH. Direct observation of conducting filaments on resistive switching of NiO thin films. Appl Phys Lett 2008;92(22):222106.

[13] Kim KM, Choi BJ, Shin YC, Choi S, Hwang CS. Anode-interface localized filamentary mechanism in resistive switching of TiO_2 thin films. Appl Phys Lett 2007;91(1):012907.

[14] Kwon DH, Kim KM, Jang JH, Jeon JM, Lee MH, Kim GH, et al. Atomic structure of conducting nanofilaments in TiO_2 resistive switching memory. Nat Nanotechnol 2010;5(2):148–53.

[15] Guan WH, Long SB, Jia R, Liu M. Nonvolatile resistive switching memory utilizing gold nanocrystals embedded in zirconium oxide. Appl Phys Lett 2007;91(6):62111.

[16] Wu X, Zhou P, Li J, Chen LY, Lv HB, Lin YY, et al. Reproducible unipolar resistance switching in stoichiometric ZrO_2 films. Appl Phys Lett 2007;90(18):183507.

[17] Chang WY, Lai YC, Wu TB, Wang SF, Chen F, Tsai MJ. Unipolar resistive switching characteristics of ZnO thin films for nonvolatile memory applications. Appl Phys Lett 2008;92(2):022110.

[18] Yang YC, Pan F, Liu Q, Liu M, Zeng F. Fully room-temperature-fabricated nonvolatile resistive memory for ultrafast and high-density memory application. Nano Lett 2009;9(4):1636–43.

[19] Stewart DR, Ohlberg DAA, Beck PA, Chen Y, Williams RS, Jeppesen JO, et al. Molecule-independent electrical switching in pt/organic monolayer/ti devices. Nano Lett 2004;4(1):133–6.

[20] Jo SH, Lu W. CMOS compatible nanoscale nonvolatile resistance switching memory. Nano Lett 2008;8(2):392–7.

[21] Sinitskii A, Tour JM. Lithographic graphitic memories. ACS Nano 2009;3(9):2760–6.

[22] Zhuge F, Dai W, He CL, Wang AY, Liu YW, Li M, et al. Nonvolatile resistive switching memory based on amorphous carbon. Appl Phys Lett 2010;96(16):163505.

[23] Eda G, Fanchini G, Chhowalla M. Large-area ultrathin films of reduced graphene oxide as a transparent and flexible electronic material. Nat Nanotechnol 2008;3(5):270–4.

[24] Cote LJ, Kim F, Huang JX. Langmuir−blodgett assembly of graphite oxide single layers. J Am Chem Soc 2009;131(3):1043–9.

[25] He CL, Zhuge F, Zhou XF, Li M, Zhou GC, Liu YW, et al. Nonvolatile resistive switching in graphene oxide thin films. Appl Phys Lett 2009;95(23):232101.

[26] Hong SK, Kim JE, Kim SO, Choi SY, Cho BJ. Flexible resistive switching memory device based on graphene oxide. IEEE Electron Dev Lett 2010;31(9):1005–7.

[27] Jeong HY, Kim JY, Kim JW, Hwang JO, Kim JE, Lee JY, et al. Graphene oxide thin films for flexible nonvolatile memory applications. Nano Lett 2010;10(11):4381–6.

[28] Zhuang XD, Chen Y, Liu G, Li PP, Zhu CX, Kang ET, et al. Conjugated-polymer-functionalized graphene oxide: synthesis and nonvolatile rewritable memory effect. Adv Mater 2010;22(15):1731–5.

[29] Liu G, Zhuang XD, Chen Y, Zhang B, Zhu JH, Zhu CX, et al. Bistable electrical switching and electronic memory effect in a solution-processable graphene oxide-donor polymer complex. Appl Phys Lett 2009;95(25):253301.

[30] Zhou XF, Liu ZP. A scalable, solution-phase processing route to ultralarge graphene sheets. Chem Commun 2010;46(15):2611–3.

[31] Lampert MA, Mark P. Current injection in solids. Academic: New York; 1970.

[32] Liu Q, Guan WH, Long SB, Jia R, Liu M. Resistive switching memory effect of ZrO_2 films with Zr^+ implanted. Appl Phys Lett 2008;92(1):012117.

[33] Inoue IH, Yasuda S, Akinaga H, Takagi H. Nonpolar resistance switching of metal/binary-transition-metal oxides/metal sandwiches: homogeneous/inhomogeneous transtion of current distribution. Phys Rev B 2008;77(3):035105.

[34] Tokunaga Y, Kaneko Y, He JP, Arima T, Sawa A, Fuji T, et al. Colossal electroresistance effect at metal electrode/$La_{1−x}Sr_{1+x}MnO_4$ interfaces. Appl Phys Lett 2006;88(22):223–507.

[35] Kund M, Beitel G, Pinnow CU, Röhr T, Schumann J, Symanczyk R, et al. Conductive bridging RAM (CBRAM): An emerging non-volatile memory technology scalable to sub 20 nm. IEDM Tech Dig (Washington DC. USA): IEEE, 2005 p 754–7.

[36] Schindler C, Meier M, Waser R. Resistive switching in Ag–Ge–Se with extremely low write currents. in: proc non-volatile memory tech symp (Albuquerque NM. USA): IEEE, 2007; 82–5.

[37] Tsunoda K, Fukuzumi Y, Jameson JR, Wang Z, Griffin PB, Nishi Y. Bipolar resistive switching in polycrystalline TiO_2 films. Appl Phys Lett 2007;90(11):113501.

[38] Banno N, Sakamoto T, Iguchi N, Sunamura H, Terabe K, Hasegawa T, et al. Diffusivity of Cu ions in solid electrolyte and its effect on the performance of nanometer-scale switch. IEEE Trans Electron Devices 2008;55(11):3283–7.

[39] Govindaraj R, Kesavamoorthy R, Mythili R, Viswanathan B. The formation and characterization of silver clusters in zirconia. J Appl Phys 2001;90(2):958–63.

[40] Li YT, Long SB, Zhang MH, Liu Q, Shao LB, Zhang S, et al. Resistive switching properties of Au/ZrO$_2$/Ag structure for low-voltage nonvolatile memory applications. IEEE Electron Device Lett 2010;31(2):117–9.

[41] Bid A, Bora A, Raychaudhuri A. Temperature dependence of the resistance of metallic nanowires of diameter $\geqslant$15 nm: applicability of Bloch–Gruneisen theorem. Phys Rev B 2006;74(3):035426.

[42] Rohde C, Choi BJ, Jeong DS, Choi S, Zhao JS, Hwang CS. Identification of a determining parameter for resistive switching of TiO$_2$ thin films. Appl Phys Lett 2005;86(26):262907.

[43] Zhou M, Wang YL, Zhai YM, Zhai JF, Ren W, Wang FA, et al. Controlled synthesis of large-area and patterned electrochemically reduced graphene oxide films. Chem–Eur J 2009;15(25):6116–20.

[44] Mativetsky JM, Treossi E, Orgiu E, Melucci M, Veronese GP, Samori P, et al. Local current mapping and patterning of reduced graphene oxide. J Am Chem Soc 2010;132(40):14130–6.

[45] Weng LS, Zhang LY, Chen YP, Rokhinson LP. Atomic force microscope local oxidation nanolithography of graphene. Appl Phys Lett 2008;93(9):093107.